

# Physical conditions in potential sources of ultra-high-energy cosmic rays: Updated Hillas plot and radiation-loss constraints

Ksenia Ptitsyna<sup>1</sup> and Sergey Troitsky<sup>2\*</sup>

<sup>1</sup> M.V. Lomonosov Moscow State University, Moscow 119992, Russia

<sup>2</sup> Institute for Nuclear Research of the Russian Academy of Sciences, 60th October Anniversary Prospect 7a, 117312, Moscow, Russia

## Abstract

We review basic constraints on the acceleration of ultra-high-energy (UHE) cosmic rays (CRs) in astrophysical sources, namely the geometrical (Hillas) criterion and restrictions from radiation losses in different acceleration regimes. Using the latest available astrophysical data, we redraw the Hillas plot and figure out potential UHECR accelerators. For the acceleration in central engines of active galactic nuclei, we constrain the maximal UHECR energy for a given black-hole mass. Among active galaxies, only the most powerful ones, radio galaxies and blazars, are able to accelerate protons to UHE, though acceleration of heavier nuclei is possible in much more abundant lower-power Seyfert galaxies.

## Contents

<b>1</b>	<b>Introduction</b>	<b>2</b>
<b>2</b>	<b>General constraints from geometry and radiation</b>	<b>3</b>
2.1	The Hillas criterion . . . . .	3
2.2	Radiation losses . . . . .	4
2.3	Different acceleration regimes . . . . .	4
2.3.1	Diffusive acceleration. . . . .	5
2.3.2	One-shot acceleration with synchrotron-dominated losses. . . . .	5
2.3.3	One-shot acceleration with curvature-dominated losses. . . . .	5
2.4	Summary of results for the maximal energy . . . . .	6
<b>3</b>	<b>Magnetic fields in particular sources</b>	<b>6</b>
3.1	Neutron stars, pulsars and magnetars . . . . .	7
3.2	Active galaxies . . . . .	7
3.2.1	Supermassive black holes and their environment. . . . .	7
3.2.2	Jets and outflows of active galaxies. . . . .	12
3.2.3	Jet knots, hot spots and lobes of powerful active galaxies. . . . .	12

---

\*st@ms2.inr.ac.ru

3.3	Star formation regions and starburst galaxies . . . . .	15
3.4	Gamma-ray bursts . . . . .	15
3.5	Galaxy clusters, superclusters and voids . . . . .	16
<b>4</b>	<b>Summary and discussion</b>	<b>17</b>
<b>5</b>	<b>Conclusions</b>	<b>23</b>
<b>A</b>	<b>Derivation of electrodynamic results</b>	<b>24</b>
A.1	Energy losses for the curvature radiation (see e.g. Ref. [88]) . . . . .	24
A.2	The maximal energy for diffusive acceleration [11] . . . . .	24

# 1 Introduction

The origin of ultra-high-energy (UHE; energy  $\mathcal{E} \gtrsim 10^{19}$  eV) cosmic rays (CRs) remains unknown despite decades of intense studies (see e.g. Ref. [1] for a comprehensive review and Ref. [2] for a recent pedagogical introduction). Recent studies, notably the observation of the Greisen–Zatsepin–Kusmin [3, 4] cutoff by the HiRes experiment [5], further supported by results of the Pierre Auger observatory (PAO) [6], suggest that at least a large fraction of UHECRs is accelerated in cosmologically distant astrophysical sources. The birth of (scientific) UHECR astronomy, however, awaits our firm understanding of energies and primary composition of the observed cosmic rays as well as identification of at least one astrophysical object where these particles are accelerated.

Given experimental ambiguities, it is important to understand theoretically, which astrophysical objects may serve as UHECR accelerators. It has been understood long ago that the UHECR sources should be distinguished objects with extreme physical conditions. One simple criterion is the geometrical one: the particle should not leave the accelerator before it gains the required energy. Presumably, the particle is accelerated by the electric field and confined by the magnetic one; then the geometrical criterion is expressed in terms of the particle’s Larmor radius which should not exceed the linear size of the accelerator (see, e.g., Ref. [7]). In the context of UHECRs, this condition is recognized as the Hillas criterion [8] and is often presented graphically in terms of the Hillas plot where the accelerator size  $R$  and the magnetic field  $B$  are plotted. We note that even quite recent reviews use either cut-and-pasted or slightly refurbished versions of the original 25-years-old plot. However, astrophysics experienced enormous progress, if not a revolution, during these decades. One of the aims of this study is to give an updated version of the Hillas plot with references to either – when possible – measurements or estimates of the magnetic fields and sizes of potential astrophysical accelerators. The most important update corresponds to a wide variety of active galaxies whose sizes and magnetic fields differ by many orders of magnitude from one object to another so that some of them may, while most of them may not, accelerate particles to UHE.

Another restriction on the cosmic-ray accelerators is posed by the radiation losses which inevitably accompany the acceleration of a charged particle. The corresponding constraints were studied, in particular, in Refs. [8, 9, 10, 11]. The radiation losses depend on the particular field configuration and the maximal achievable energy of a particle in the loss-limited regime depends on the acceleration mechanism. Restricting to particular mechanisms or particular field configurations may result in would-be contradictory results, cf. Refs. [10, 11]. In this work, we review the radiation-loss constraint for different cases; they further limit the acceptable region on the updated

Hillas plot. One of possible applications of these general constraints is a study of active galaxies correlated with the Auger events [12].

One should always keep in mind that even if both geometric and radiation constraints are satisfied, they do not yet guarantee particle acceleration to the corresponding energy. Each particular source should be discussed in the context of an acceleration mechanism operating there.

The rest of the paper is organised as follows. In Sec. 2, we review constraints on potential UHE accelerators, that is model-independent Hillas geometrical constraint and limitations due to radiation losses for particular acceleration mechanisms. In Sec. 3, we take advantage of the modern astrophysical data and redraw the Hillas plot supplemented by the radiation-loss constraints. Our results are summarized and discussed in Sec. 4 while brief conclusions are given in Sec. 5. Appendix A contains derivation of some formulae.

## 2 General constraints from geometry and radiation

An accelerator of UHECR particles should satisfy several general constraints which may be briefly summarized as follows:

- **geometry** — the accelerated particle should be kept inside the source while being accelerated;
- **power** — the source should possess the required amount of energy to give it to accelerated particles;
- **radiation losses** — the energy lost by a particle for radiation in the accelerating field should not exceed the energy gain;
- **interaction losses** — the energy lost by a particle in interactions with other particles should not exceed the energy gain;
- **emissivity** — the total number (density) and power of sources should be able to provide the observed UHECR flux;
- **accompanying radiation** of photons, neutrinos and low-energy cosmic rays should not exceed the observed fluxes, both for a given source and for the diffuse background (in particular, the ensemble of sources should reproduce the observed cosmic-ray *spectrum*<sup>1</sup>).

The primary concern of this paper is the geometrical and radiation-loss constraints (others are briefly quoted when relevant); both restrict the magnetic field and the size of the accelerator and can be graphically represented on the Hillas plot.

### 2.1 The Hillas criterion

The Larmor radius  $R_L$  of a particle does not exceed the accelerator size, otherwise the particle escapes the accelerator and cannot gain energy further. This Hillas criterion sets the limit

$$\mathcal{E} \leq \mathcal{E}_H = qBR \quad (1)$$

for the energy  $\mathcal{E}$  gained by a particle with charge  $q$  in the region of size  $R$  with the magnetic field  $B$ .

---

<sup>1</sup>We note that the spectrum of cosmic rays accelerated in a particular source may be very different from the spectrum observed at the Earth, cf. Ref. [13].

## 2.2 Radiation losses

While Eq. (1) is a necessary limit, more stringent ones may arise from the energy losses: the maximal energy  $\mathcal{E}_{\text{loss}}$  a particle can get in an accelerator of infinite size is determined by the condition

$$\frac{d\mathcal{E}^{(+)}}{dt} = -\frac{d\mathcal{E}^{(-)}}{dt}, \quad (2)$$

where the energy gain rate in the effective electric field  $E = \eta B$  is (in the particle-physics  $c = 1$  units which we use throughout the paper)

$$\frac{d\mathcal{E}^{(+)}}{dt} = q\eta B \quad (3)$$

(kept explicit in equations, the efficiency coefficient  $\eta$  is set to one in figures to obtain conservative (optimistic) limits for a given magnetic field – the electric fields in astrophysical objects are much less studied observationally compared to the magnetic ones, but it is always expected that  $E \ll B$ ). Depending on particular conditions in the accelerator, the maximal energy  $\mathcal{E}_{\text{max}}$  of a particle is limited either by geometrical or by energy-loss arguments:

$$\mathcal{E}_{\text{max}} = \min \{ \mathcal{E}_{\text{H}}, \mathcal{E}_{\text{loss}} \}.$$

The general expression for total radiation losses for a particle with velocity  $\mathbf{v}$  moving in arbitrary electric  $\mathbf{E}$  and magnetic  $\mathbf{B}$  fields reads (see e.g. Ref. [14])

$$-\frac{d\mathcal{E}^{(-)}}{dt} = \frac{2}{3} \frac{q^4}{m^4} \mathcal{E}^2 \left( (\mathbf{E} + [\mathbf{v} \times \mathbf{B}])^2 - (\mathbf{E} \cdot \mathbf{v})^2 \right), \quad (4)$$

where  $q$  and  $m$  are the particle's charge and mass; cross and dot denote vector and scalar product, respectively. By making use of relativistic equations of motion, Eq. (4) can be conveniently rewritten [15] as

$$-\frac{d\mathcal{E}^{(-)}}{dt} = \frac{2}{3} \frac{q^2}{m^2(1-v^2)} \left( \mathbf{F}^2 - (\mathbf{F} \cdot \mathbf{v})^2 \right).$$

The force  $\mathbf{F}$  acting on a particle is further decomposed as  $\mathbf{F} = \mathbf{F}_{\parallel} + \mathbf{F}_{\perp}$ , where we determine the parallel  $\mathbf{F}_{\parallel}$  and perpendicular  $\mathbf{F}_{\perp}$  components with respect to  $\mathbf{v}$ , that is  $(\mathbf{F}_{\perp} \cdot \mathbf{v}) = 0$ . Then

$$-\frac{d\mathcal{E}^{(-)}}{dt} = \frac{2}{3} \frac{q^2}{m^2(1-v^2)} \left( F_{\perp}^2 + F_{\parallel}^2(1-v^2) \right). \quad (5)$$

It is apparent that the second term (the so-called curvature radiation) is suppressed with respect to the first one (synchrotron radiation) by an extra power of  $(1-v^2)$  and therefore may be neglected in the ultrarelativistic regime unless the synchrotron term is zero or very small itself. The synchrotron losses are dominant for any generic field configuration; however, in a very specific regime  $\mathbf{v} \parallel \mathbf{E} \parallel \mathbf{B}$  they vanish, and the losses are then determined by the curvature radiation.

## 2.3 Different acceleration regimes

Depending on the scenario of acceleration, we will consider diffusive (stochastic) and inductive (one-shot, or direct) mechanisms (see e.g. Ref. [8] for a general discussion of these two approaches to UHECR acceleration).

The prime examples of diffusive processes are the Fermi first-order [16] and second-order (shock, e.g. [17]) acceleration. Other possibilities include interaction with medium by crossing a boundary between layers with different velocities [18] and even transformation of a particle into a different one [19]. A recent review and more references can be found in Ref. [20].

In inductive mechanisms, the particle is accelerated by the large-scale electric field continuously and then leaves the accelerator. Strong ordered fields on relatively large scales are required; example scenarios are given e.g. in Refs. [21, 22, 23, 24, 25]. For our purposes, it is convenient to separate the inductive-acceleration scenarios into two groups, depending on whether the configuration of the accelerating field corresponds to synchrotron- (e.g. large-scale jets [21]) or curvature-dominated (neutron stars [22] and black holes [23, 24, 25]) losses.

### 2.3.1 Diffusive acceleration.

The losses in this regime are the most serious. This scenario cannot be realized in strongly ordered field configurations with  $\mathbf{v} \parallel \mathbf{E} \parallel \mathbf{B}$ , therefore the losses are determined by the synchrotron limit,

$$-\frac{d\mathcal{E}^{(-)}}{dt} = \frac{2}{3} \frac{q^2}{R_L^2} \left( \frac{\mathcal{E}}{m} \right)^4 = \frac{2}{3} \frac{q^4}{m^4} \mathcal{E}^2 B^2 \quad (\text{synchrotron}). \quad (6)$$

This regime has been studied in Ref. [11] where it has been shown (see Appendix A.2) that the maximal energy is limited by

$$\mathcal{E}_d \simeq \frac{3}{2} \frac{m^4}{q^4} B^{-2} R^{-1}. \quad (7)$$

Diffusive mechanisms are quite generic and may work in every realistic environment which can host, e.g., a shock wave. Eq. (7) does not rely on a particular acceleration mechanism and gives a (hardly reachable) upper limit for the maximal energy.

### 2.3.2 One-shot acceleration with synchrotron-dominated losses.

In this regime, the energy loss rate is given by Eq. (6) and, given Eq. (3), Eq. (2) results in the maximal energy

$$\mathcal{E}_s = \sqrt{\frac{3}{2}} \frac{m^2}{q^{3/2}} B^{-1/2} \eta^{1/2}. \quad (8)$$

This acceleration mechanism requires ordered fields throughout the acceleration site; its practical realization for UHECR may work in jets of powerful active galaxies [21].

### 2.3.3 One-shot acceleration with curvature-dominated losses.

The energy loss rate is determined (see Appendix A.1) by

$$-\frac{d\mathcal{E}^{(-)}}{dt} = \frac{2}{3} \frac{q^2}{r^2} \left( \frac{\mathcal{E}}{m} \right)^4 \quad (\text{curvature}), \quad (9)$$

where  $r$  is the curvature radius of the field lines which is supposed to be of order of the accelerator size and Eq. (2) results in the maximal energy

$$\mathcal{E}_c = \left( \frac{3}{2} \right)^{1/4} \frac{m}{q^{1/4}} B^{1/4} R^{1/2} \eta^{1/4}. \quad (10)$$

This mechanism requires ordered fields of very specific configurations which, however, may be present in the immediate vicinity of neutron stars and black holes [22, 23, 24, 25].

## 2.4 Summary of results for the maximal energy

Let us summarize the expressions for the maximal energy  $\mathcal{E}_{\max}$  (in the comoving frame) attainable by a nuclei with atomic number  $Z$  and mass  $A$  in the accelerator of size  $R$  filled with magnetic field  $B$ , for different acceleration regimes:

$$\mathcal{E}_{\max}(B, R) = \begin{cases} \mathcal{E}_{\text{H}}(B, R), & B \leq B_0(R); \\ \mathcal{E}_{\text{loss}}(B, R), & B > B_0(R), \end{cases}$$

where

$$B_0(R) = 3.16 \times 10^{-3} \text{ G} \frac{A^{4/3}}{Z^{5/3}} \left( \frac{R}{\text{kpc}} \right)^{-2/3} \eta^{1/3},$$

is determined from Eqs. (1) and (7), (8) or (10) by requiring  $\mathcal{E}_{\text{H}}(B, R) = \mathcal{E}_{\text{loss}}(B, R)$ ; the Hillas constraint is

$$\mathcal{E}_{\text{H}}(B, R) = 9.25 \times 10^{23} \text{ eV } Z \left( \frac{R}{\text{kpc}} \right) \left( \frac{B}{\text{G}} \right)$$

and the radiation-loss constraints are

$$\mathcal{E}_{\text{loss}}(B, R) = \mathcal{E}_{\text{d}}(B, R) = 2.91 \times 10^{16} \text{ eV } \frac{A^4}{Z^4} \left( \frac{R}{\text{kpc}} \right)^{-1} \left( \frac{B}{\text{G}} \right)^{-2}$$

for diffusive acceleration,

$$\mathcal{E}_{\text{loss}}(B, R) = \mathcal{E}_{\text{s}}(B, R) = 1.64 \times 10^{20} \text{ eV } \frac{A^2}{Z^{3/2}} \left( \frac{B}{\text{G}} \right)^{-1/2} \eta^{1/2}$$

for inductive acceleration with synchrotron-dominated losses and

$$\mathcal{E}_{\text{loss}}(B, R) = \mathcal{E}_{\text{c}}(B, R) = 1.23 \times 10^{22} \text{ eV } \frac{A}{Z^{1/4}} \left( \frac{R}{\text{kpc}} \right)^{1/2} \left( \frac{B}{\text{G}} \right)^{1/4} \eta^{1/4}$$

for inductive acceleration with curvature-dominated losses. Applications to particular objects and graphical representations of the constraints will follow in Sec. 4 (see in particular Figs. 8 – 12).

Note that the critical value  $B_0(R)$ , at which  $\mathcal{E}_{\text{H}}(B, R) = \mathcal{E}_{\text{loss}}(B, R)$ , is the same for all three acceleration regimes: in this case, the Larmor radius  $R_L$  and the size of the accelerator  $R$  are equal; within our approximation they coincide also with the curvature radius  $r$  of the field lines. Therefore the diffusive acceleration regime merges the one-shot acceleration because the particle interacts with the shock wave only once in this limiting case; moreover, Eqs. (6) and (9) coincide and the two regimes of inductive acceleration result in similar losses.

## 3 Magnetic fields in particular sources

A number of astrophysical sources have been proposed where acceleration of cosmic rays up to the highest energies can take place (see e.g. Refs. [26, 27] for reviews and summary). In this section, we review experimental information on their magnetic fields in order to put them in proper places on the Hillas plot. General methods of astrophysical magnetic-field studies are discussed e.g. in Refs. [28, 29]; however, a much wider variety of them is used for studies of individual sources.

### 3.1 Neutron stars, pulsars and magnetars

Neutron stars host the highest known magnetic fields in the Universe. In particular, magnetars (including anomalous X-ray pulsars) may possess kilometer-scale fields  $B \sim 10^{14}$  G and higher while normal neutron stars have  $B \sim (10^{11} \div 10^{12})$  G. Observational evidence for these high fields is discussed e.g. in Sec. 6.3 of Ref. [30]. We note also a direct (though not widely accepted) observational method to measure  $B$  in neutron stars, observation of spectral lines giving evidence for resonant Compton scattering at cyclotron frequency in the high-field media, see e.g. Ref. [31] for normal neutron stars and Ref. [32] for anomalous X-ray pulsars.

### 3.2 Active galaxies

For the purposes of the present study, we will use a simplified classification of active galaxies (see textbooks [33, 34] and, for a more detailed discussion, Ref. [35]). Clearly, there are many intermediate states and peculiar objects which do not fit this classification well; while they should be studied individually if suspected to be UHECR sources, their parameters of relevance (sizes and magnetic fields) are expected to interpolate between those of better classified active galaxies.

**Seyfert galaxies** – spiral galaxies with bright emission-line nuclei; radio-weak; do not possess large-scale relativistic jets; often have starburst activity.

**Radio galaxies** – radio-loud elliptical galaxies with relativistic jets. According to Ref. [36], they are classified into two luminosity classes: FR I (less powerful; jets brighter towards core; jets may be curved) and FR II (most powerful; straight jets brighter at the hot spots at their end points).

**Blazars** – (almost) point-like objects with non-thermal spectrum; strongly variable; similar in total power to radio galaxies; may be associated with radio galaxies whose jets are pointed towards the observer. They may be divided into BL Lac type objects (relatively low power; no emission lines; possible counterparts of FR I radio galaxies) and optically violently variable quasars (extremely powerful; may have emission lines; possible counterparts of FR II).

Low-power active galaxies (Seyferts) are much more abundant than radio galaxies and blazars.

Possible acceleration sites in active galaxies include both the central engine (immediate vicinity of the black hole and the accretion disk) and extended structures (jets, lobes, hot spots and jet knots). We will discuss separately the black-hole environment and extended structures because of very different conditions for particle acceleration. Let us note that the term “active galactic nuclei” (AGN) is often used to describe a region much larger than just the black hole and its accretion disc and often includes inner jets (or sometimes even larger structures) which we consider separately.

#### 3.2.1 Supermassive black holes and their environment.

Measurements of magnetic fields in the central regions of galaxies have been performed by means of the following methods (see Fig. 1 for particular results).

**1. Synchrotron self-absorption.** Under certain conditions, the low-energy cutoff in the spectrum of a compact source may be detected and its shape may be proven to correspond to the absorption of synchrotron photons on themselves. If this is the case, then the magnetic-field strength may be determined by means of the Slyph formula [45] or its modifications. The method works best of all for strong radio sources with resolved nuclear components [41, 42, 43, 44].

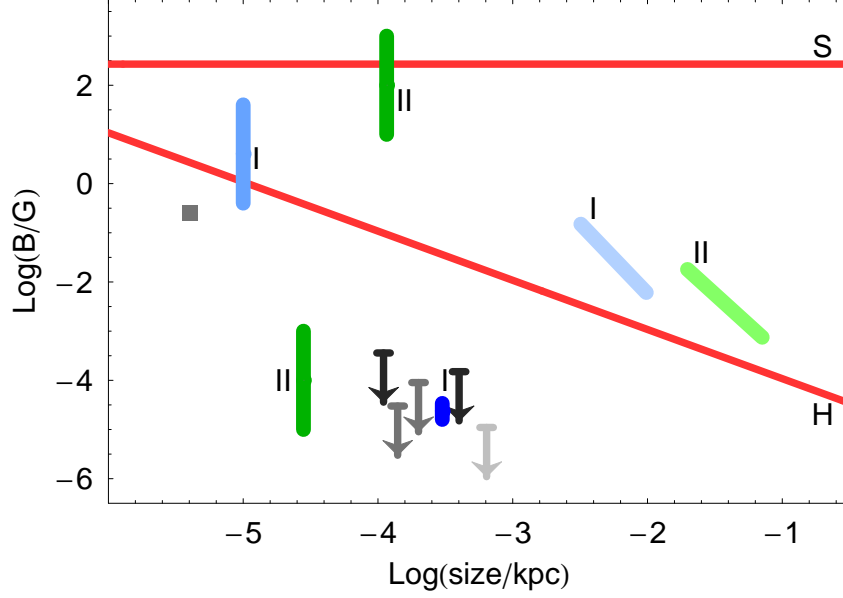


Figure 1: The size-field diagram for central regions of active galactic nuclei. Grey colors (box and arrows) correspond to Seyfert galaxies, blue colors (error-bar lines marked I) correspond to FRI radio galaxies, green colors (error-bar lines marked II) correspond to FR II radio galaxies and quasars. Arrows: upper limits from the Zeeman splitting in megamasers (light grey, Ref. [37]; medium grey, Ref. [38]; dark grey, Ref. [39]). Dark blue (I) vertical error bar: Faraday rotation measurements, Ref. [40]. The grey box [41], light blue (I) vertical [42], dark green (II) [43] and diagonal (I and II) [44] error bars correspond to the measurements by the synchrotron self-absorption method (see text). The allowed region for acceleration of  $10^{20}$  eV protons is located between thick red lines H and S (the lower line, H, corresponds to the Hillas limit; the upper one, S, corresponds to the radiation-loss limit for one-shot acceleration with synchrotron-dominated losses).

**2. Polarimetry.** Measurements of the Faraday rotation and of resulting depolarization give estimates of the magnetic field provided the plasma density is known from independent observations [40].

**3. Zeeman effect in megamasers.** Megamasers are compact sources of coherent radiation in molecular clouds inside or around the accretion disk. Current precision allows to put very stringent constraints on the magnetic fields in these regions from non-observation of the Zeeman splitting in megamasers in nearby Seyfert galaxies [37, 38, 39].

**4. The iron  $K_\alpha$  line.** Measurements of the width and shape of this X-ray line may provide important information about circumnuclear dynamics; in particular, it may be used to estimate the magnetic field, though present constraints are quite weak [46].

All these direct measurements, however, cannot probe the most interesting region in the immediate vicinity of the central black hole, a few Schwarzschild radii ( $R_S$ ) from the center. This region is particularly important because theoretically motivated configurations of electric and magnetic fields may allow for negligible synchrotron radiation of accelerated particles and thus for (relatively weak) curvature-radiation losses. Lack of our understanding of the field structure in the accretion disk is transformed into uncertainties in the inferred magnetic fields  $B_{\text{BH}}$  at the black-hole horizon (see e.g. Ref. [47] for a summary of models used for this extrapolation). Direct estimates of  $B_{\text{BH}}$  are therefore not only scarce but also model-dependent.

On the other hand, parameters of the environment of a black hole and in particular the value of  $B_{\text{BH}}$  depend strongly on the black-hole mass  $M_{\text{BH}}$ . A conservative upper limit on  $B_{\text{BH}}$  follows from the condition that the maximal rate of extraction of the rotational energy of a black hole does not exceed the Eddington luminosity [48] (see Ref. [49] for a detailed discussion),

$$B_{\text{BH}} \lesssim 3.2 \times 10^8 \left( \frac{M_{\text{BH}}}{M_\odot} \right)^{-1/2} \text{ G}. \quad (11)$$

Quite old but popular models estimate the  $M_{\text{BH}} - B_{\text{BH}}$  relation from the pressure balance (radiation pressure equals to the magnetic-viscosity pressure) [50, 51]:

$$B_{\text{BH}} \sim 10^8 \left( \frac{M_{\text{BH}}}{M_\odot} \right)^{-1/2} \text{ G}. \quad (12)$$

An efficient method to constrain the relation between  $M_{\text{BH}}$  and  $B_{\text{BH}}$  was found in Ref. [52] in the frameworks of a particular (not generally accepted) theoretical model in which both  $M_{\text{BH}}$  and  $B_{\text{BH}}$  are related to the observable luminosity at 5100 Å. It gives somewhat lower values of  $B_{\text{BH}}$  than Eq. (12); the best fit is

$$\log \left( \frac{B_{\text{BH}}}{\text{G}} \right) = (9.26 \pm 0.39) - (0.81 \pm 0.05) \log \left( \frac{M_{\text{BH}}}{M_\odot} \right), \quad (13)$$

where the central values of the coefficients are taken from Ref. [52] and the error bars are estimated by us from their data. For two cases when rather firm and model-independent values of  $B_{\text{BH}}$  could be inferred from the observations (synchrotron self absorption measured at different radii down to 0.1 pc and extrapolated to  $R_S$ , Ref. [44]), we estimated the corresponding  $M_{\text{BH}}$  and found that both values are in a good agreement with Eq. (13), though precision is quite low.

Estimates of  $B_{\text{BH}}$  versus  $M_{\text{BH}}$  are summarized in Fig. 2. We will use the upper limit, Eq. (11), to estimate  $B_{\text{BH}}$  for a given  $M_{\text{BH}}$ ; we note however that realistic values of  $B_{\text{BH}}$  are 1...2 orders of magnitude lower. Since for the curvature-dominated radiation

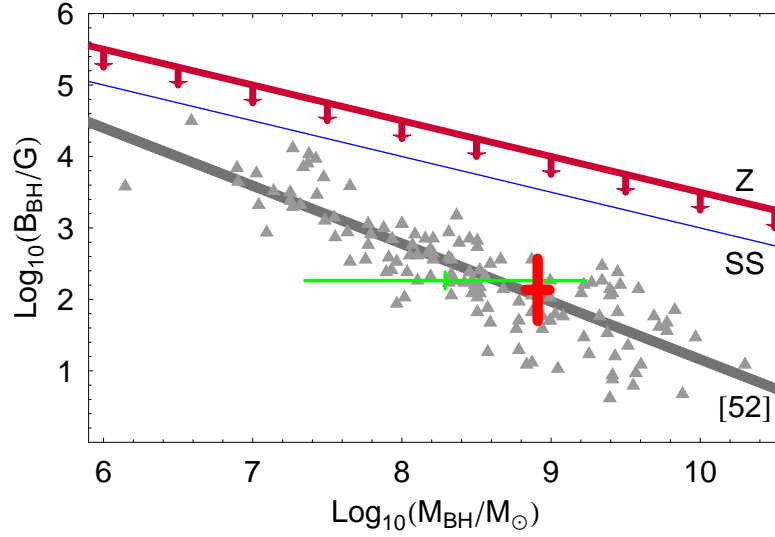


Figure 2: Magnetic field  $B_{\text{BH}}$  at the black-hole horizon versus the black hole mass  $M_{\text{BH}}$ . Triangles are estimates of Ref. [52] (determined in the frameworks of a particular, not generally accepted model) and the grey line (marked [52]) represents their best fit, Eq. (13). Two points with error bars correspond to experimental estimates of  $B_{\text{BH}}$ , Ref. [44], using the synchrotron self-absorption method ( $M_{\text{BH}}$  estimated by us using the stellar velocity dispersion from HyperLEDA [53] (thick dark red, FRI radio galaxy 3C 465) and 2MASS  $K_s$  magnitude quoted in NED [54] (thin light green, FRII radio galaxy 3C 111); see Ref. [12] for details). Thin blue line (SS) corresponds to the Shakura–Sunyaev estimate, Eq. (12). Thick red line (Z) represents the Znajek upper limit, Eq. (11). This conservative upper limit is used in our estimates of the maximal cosmic-ray energy.

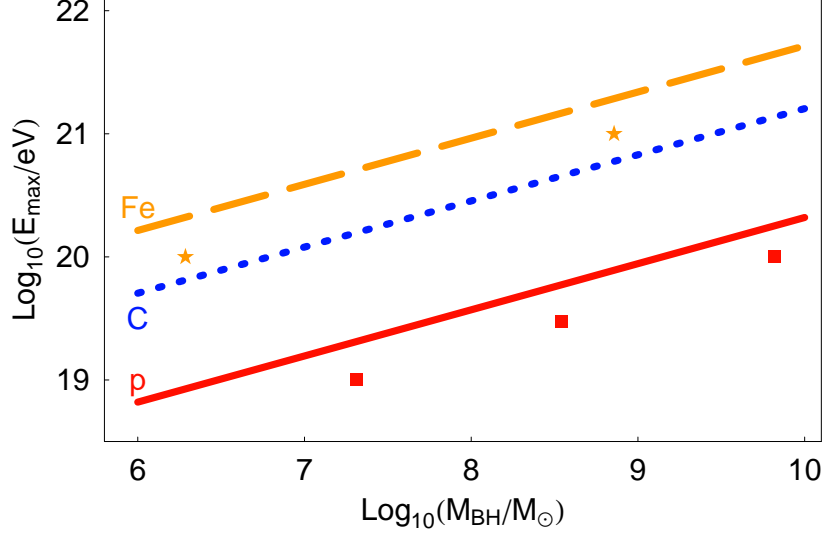


Figure 3: Upper limit on the maximal attainable energy of protons (red solid line), carbon nuclei (blue dotted line) and iron nuclei (orange dashed line) for acceleration with curvature-dominated losses near a supermassive black hole, Eq. (15). The maximal energy obtained in numerical simulations in a particular mechanism [25] is shown by red boxes (protons) and orange stars (iron nuclei); these data were obtained from Figs. 5 and 10 of Ref. [25] and Eq. (11) of this paper.

losses higher  $B$  always results in higher  $\mathcal{E}_{\max}$ , this assumption is conservative for our purposes.

The size  $R$  of the potential acceleration region (that is, the region occupied by  $\mathbf{E} \parallel \mathbf{B}$  fields suitable for curvature-dominated losses) is of order  $R_S$ ; therefore both  $R$  and  $B$  are governed by a single parameter  $M_{\text{BH}}$ , so one may express the maximal energy through  $M_{\text{BH}}$  using results of Sec. 2.4. Assuming

$$R \sim 5R_S \approx 5 \times 10^{-5} \text{ pc } \frac{M_{\text{BH}}}{10^8 M_{\odot}}, \quad (14)$$

one finds that for any reasonable  $M_{\text{BH}}$  (ranging from  $\sim 10^6 M_{\odot}$  for normal galaxies through  $(10^7 \dots 10^8) M_{\odot}$  for Seyfert galaxies to  $(10^9 \dots 10^{10}) M_{\odot}$  for powerful radio galaxies and quasars) the maximal energy is determined by radiation losses rather than by the Hillas condition and equals to

$$\mathcal{E}_{\max} = \mathcal{E}_c \simeq 3.7 \times 10^{19} \text{ eV } \frac{A}{Z^{1/4}} \left( \frac{M_{\text{BH}}}{10^8 M_{\odot}} \right)^{3/8}. \quad (15)$$

This general constraint is presented in Fig. 3 for different nuclei ( $A, Z$ ); for comparison, results of numerical simulations of particle acceleration near a supermassive black hole [25] are also plotted.

In a way similar to other observational manifestations of supermassive black holes, both details of cosmic-ray acceleration and radiation losses may depend on the accretion rate, accretion mode, environment etc. However, we are interested here in the upper limit on the maximal attainable energy of a cosmic-ray particle which is determined by  $M_{\text{BH}}$  as we have just demonstrated.

### 3.2.2 Jets and outflows of active galaxies.

Active galactic nuclei fuel large-scale (from sub-parsec to kiloparsec and even Megaparsec length) extended more or less linear jets. Revolutionary progress in the angular resolution of radio (sub-milliarcsecond) and X-ray (sub-arcsecond) imaging allowed for detailed studies and modelling of physical conditions in jets. We briefly review basics of the current understanding of jet properties following Refs. [55, 56].

Seyfert galaxies possess extended structures which are often non-collimated (opening angle of  $45^\circ$  or more) and are found to be non-relativistic; they are sometimes determined as “outflows”, reserving the term “jets” to strongly collimated relativistic flows. X-ray emission from these outflows, when present, is well described by thermal radiation (sometimes associated with star-forming regions in the outflow [57]).

Relativistic jets reveal themselves in non-thermal X-ray emission studied now in great detail. The jets are spatially resolved into components; in nearby jets (Cen A) inner and outer layers and bright knots are resolved. It is often assumed that all jets are fuelled by the central black hole; the energy flux is dominated by the magnetic-field energy at sub-parsec scales but becomes particle-dominated at parsec scales. The emission of low-luminosity sources (FR I radio galaxies and BL Lacs) is adequately described by the synchrotron models from radio to X rays; their jets are decelerated by entrainment of gas and dissipate in the end. High-power FR II and quasar jets bring their energy flux directly to their terminal hot spots and require additional (e.g. Compton) component to describe their spectra. Comparison of radio to X-ray observations gives rather firm evidence to the origin of the emission of FR I jets from accelerated particles and to acceleration of these particles not only in a finite number of shocks but also by means of some distributed mechanism along the jet [58, 59]. Quite rarely, relativistic jets are present in exceptionally powerful Seyfert galaxies; in these cases, they have properties very similar to FR I jets [56]. Models of multifrequency spectra allow to constrain the magnetic field, the key parameter of the synchrotron radiation. The estimates depend also on the electron density; the degeneracy is often removed either by the equipartition assumption or by a simultaneous measurement of the self-Compton component, when applicable. When error bars are given, they include the corresponding uncertainties. Some of these estimates [56, 60, 61, 62, 63] are presented in Fig. 4. In some cases, existence of ordered fields through the jet was proven, so that the inductive acceleration may be possible (see e.g. Ref. [21]).

### 3.2.3 Jet knots, hot spots and lobes of powerful active galaxies.

When a relativistic jet is present, it may be accompanied by internal shock regions (knots), terminal shock regions (hot spots) and extended regions in the intergalactic space fuelled by the jet after its termination (lobes). These regions are typically absent in low-power active galaxies (Seyfert galaxies): knots are observed mostly in jets of FR I radio galaxies and quasars, lobes are typical for radio galaxies, hot spots are present in the most powerful FR II radio galaxies and quasars. Magnetic fields may be determined either by X-ray synchrotron observations alone (assuming equipartition) or by combined multifrequency observations of both synchrotron and Compton radiations (allowing to relax the equipartition assumption which occurs, in the end, a good approximation, see e.g. Ref. [64])<sup>2</sup>. A summary of measurements [66, 67, 68] is given in Fig. 5.

---

<sup>2</sup>An interesting approach to determination of the magnetic field in a knot in M87 [65] exploits the energy dependence of the energy loss rate, assuming it is synchrotron-dominated. The resulting  $\sim 0.6$  mG field is in a good agreement with equipartition-based estimates.

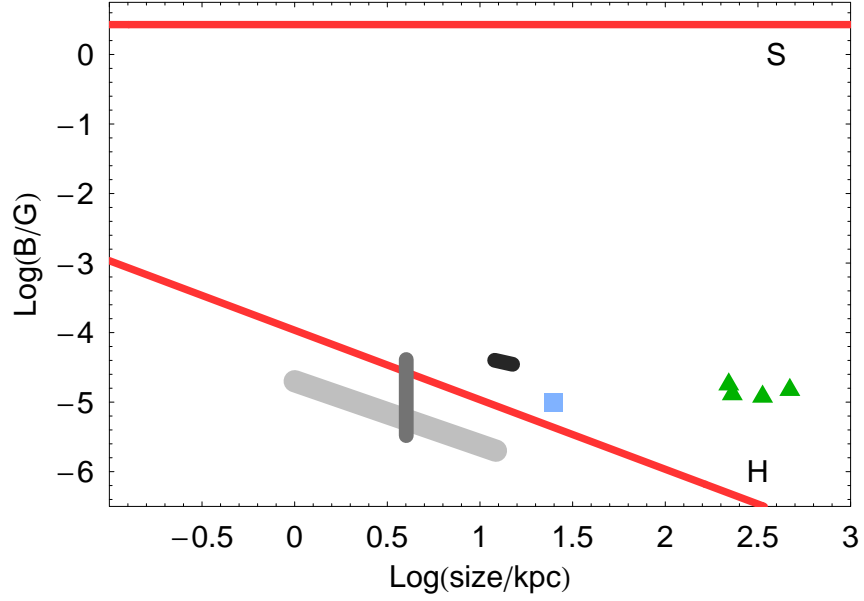


Figure 4: The size-field diagram for jets and outflows of individual active galaxies. Grey colors correspond to Seyfert galaxies, data from Refs. [56] (light-grey diagonal line), [60] (grey vertical error bar), [61] (short dark grey diagonal). Blue box corresponds to FR I radio galaxy [62]; green triangles represent quasar jets [63]. The allowed region for acceleration of  $10^{20}$  eV protons is located between thick red lines H and S (the lower line, H, corresponds to the Hillas limit; the upper one, S, corresponds to the radiation-loss limit for inductive acceleration with synchrotron-dominated losses).

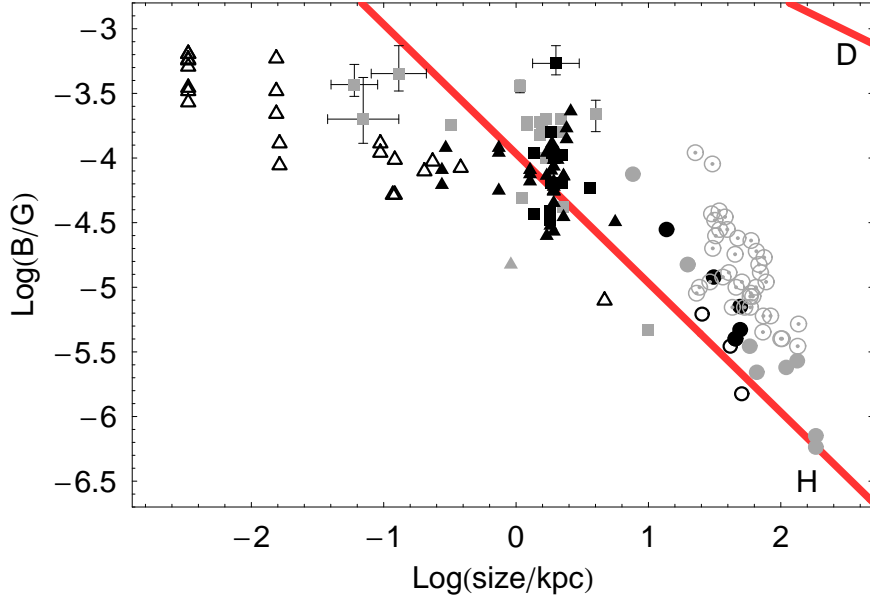


Figure 5: The size-field diagram for knots (triangles), hot spots (boxes) and lobes (circles) of individual powerful active galaxies. Filled black symbols correspond to quasars and blazars, filled grey symbols correspond to FR II radio galaxies, empty symbols correspond to FR I radio galaxies (data from Ref. [66], X-ray observations assuming equipartition); boxes with error bars represent the “best-guess” estimates of Ref. [67]; dotted grey circles correspond to FR II lobes studied in Ref. [68] (comparison of radio and X-ray observations without the equipartition assumption). The allowed region for acceleration of  $10^{20}$  eV protons is located between thick red lines H and D (the lower line, H, corresponds to the Hillas limit; the upper one, D, corresponds to the radiation-loss limit for diffusive acceleration).

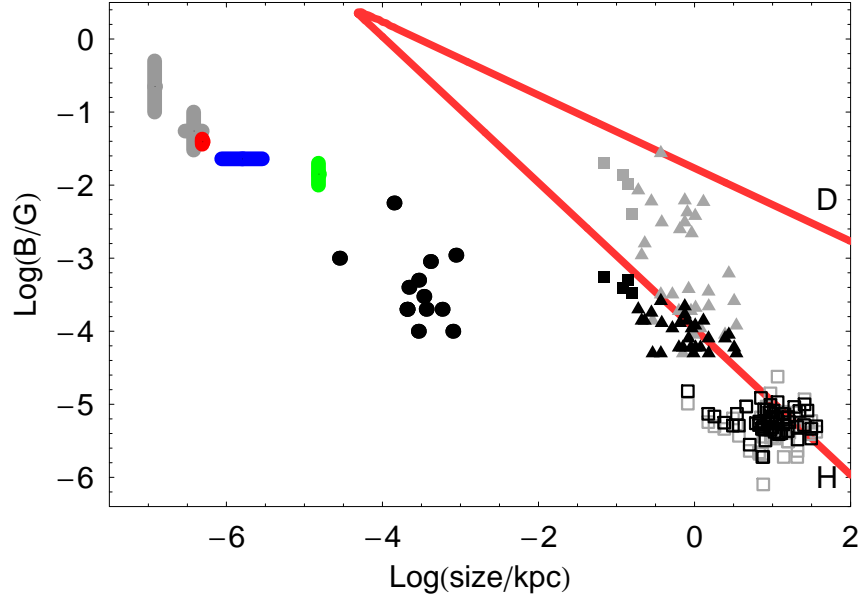


Figure 6: The size-field diagram for Galactic star-forming regions ( $R \lesssim \text{pc}$ ) and starburst galaxies ( $R \gtrsim 0.1 \text{ kpc}$ ). Thick (error-bar) lines correspond to measurements of the Zeeman splitting in masers (grey, Ref. [69]; red, Ref. [70]; blue, Ref. [71]; green, Ref. [72]). Black dots represent results of submillimeter imaging polarimetry of Ref. [73]. Data for normal (empty boxes), starburst (triangles) and extreme starburst (filled boxes) galaxies are taken from Ref. [75]; black symbols correspond to the minimal-energy field estimates while grey symbols correspond to equipartition field estimates. The allowed region for acceleration of  $10^{20} \text{ eV}$  protons is located between thick red lines H and D (the lower line, H, corresponds to the Hillas limit; the upper one, D, corresponds to the radiation-loss limit for diffusive acceleration).

### 3.3 Star formation regions and starburst galaxies

Measurements of the magnetic field in Galactic star-forming regions becomes possible with the Zeeman splitting in masers in circumstellar disks [69, 70, 71, 72] and infrared imaging polarimetry [73]. Though these regions in our Galaxy have never been considered as possible sites of UHECR acceleration, these measurements may give some hints to the fields in larger star-forming regions in starburst galaxies, where particles could be accelerated to very high energies e.g. in shocks from subsequent supernova explosions [74]; magnetic fields in these extragalactic sites are measured indirectly. A summary of measurements is given in Fig. 6; a number of arguments in favour of higher (equipartition) fields in starburst galaxies were presented in Ref. [75] while continuity (see Fig. 6) with the Galactic measurements may support lower (minimal-energy) estimates.

### 3.4 Gamma-ray bursts

Estimates of the magnetic field in gamma-ray bursts (GRBs) assume [76] that the origin of both prompt and afterglow emissions in a certain part of the spectrum is the synchrotron radiation of relativistic electrons. This assumption is supported by measurements of the afterglow spectra and lightcurves and by observation of the strongly

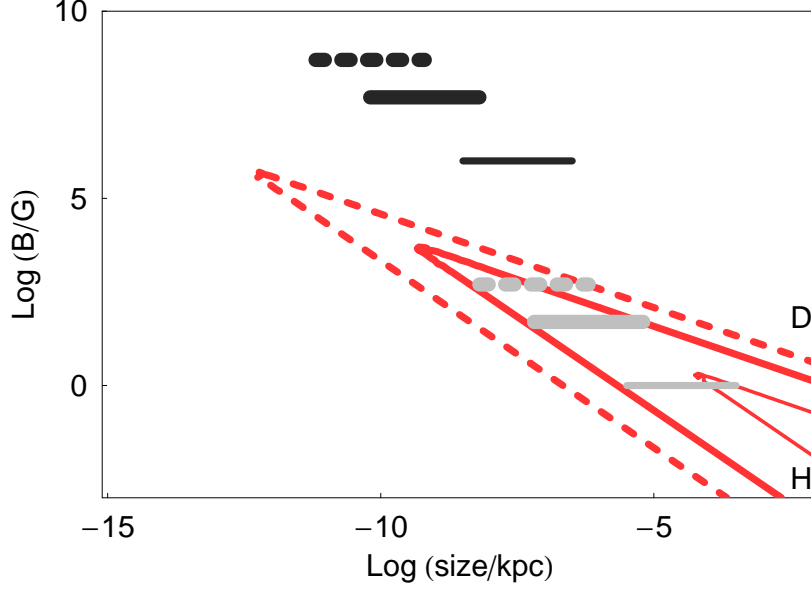


Figure 7: The size-field diagram for gamma-ray bursts. Horizontal lines represent estimates of Ref. [76] which assume the synchrotron origin for the prompt emission (dark grey) and the afterglow (light grey). The allowed region for acceleration of  $10^{20}$  eV protons is located between (the lower lines, H, correspond to the Hillas limit; the upper ones, D, correspond to the radiation-loss limit for diffusive acceleration). Dashed lines assume  $\Gamma = 500$ , thick lines assume  $\Gamma = 50$ , thin lines assume  $\Gamma = 1$ .

polarized prompt emission (see Ref. [76] for discussion and references). Ref. [76] quotes  $B \sim 10^6$  G for  $R \sim (10^{13} \div 10^{15})$  cm (prompt emission) and  $B \sim 1$  G for  $R \sim (10^{16} \div 10^{18})$  cm (afterglow) (we assume that the estimates correspond to the observer's rest frame). Another, somewhat higher field estimate may be obtained following Ref. [10] (see also Ref. [77]) from the total luminosity of a GRB, assuming that the magnetic-field energy  $\mathcal{E}_m$  is a fraction  $\epsilon_m < 1$  of the radiation energy  $\mathcal{E}_{\text{rad}}$ . However, this estimate depends strongly on the assumed beaming.

Within the scope of this paper, we may estimate the maximal energy  $\mathcal{E}_{\text{max}}$  of accelerated particles in the comoving frame following equations of Sec. 2.4 for shock (diffusive) acceleration. The GRB shells are however ultrarelativistic ( $\Gamma \sim 100$ , see e.g. Ref. [78]) and we have to multiply the comoving-frame  $\mathcal{E}_{\text{max}}$  by  $\Gamma$  to get the maximal rest-frame energy. Results are presented in Fig. 7 which, for the GRB case, is more instructive than the summary plots of Sec. 4. We note that at large  $\Gamma$ , the maximal energy may be limited by interactions with thermal photon field (not taken into account in the present work) and *decreases* as  $\Gamma^{-1}$  at large  $\Gamma$  [10].

### 3.5 Galaxy clusters, superclusters and voids

Information about cluster magnetic fields comes mostly from observations of their extended radio, and sometimes X-ray, emission. These observations are reviewed e.g. in Refs. [28, 79, 80], where more references to original works may be found. Estimates based on equipartition (see e.g. Refs. [81, 82]), as well as those assuming Compton scattering on CMB photons, favour values of  $B \sim (0.1 \div 1) \mu\text{G}$  at megaparsec scales; Faraday rotation measurements (see e.g. Refs. [83, 84, 85]) favour somewhat higher fields,

$B \sim (1 \div 5) \mu\text{G}$ . Model-dependent numerical simulations remain the main source of information about magnetic fields at the supercluster scales ( $R \sim 100 \text{ Mpc}$ ), especially in voids. Estimates vary between  $B \sim 10^{-11} \text{ G}$  [86] and  $B \sim 10^{-8} \text{ G}$  [87].

## 4 Summary and discussion

Based on the data collected in Sec. 3 and on the limits on the maximal energy, Sec. 2.4, we redraw here the Hillas plot supplemented by radiation-loss constraints. Figures 8 – 10 give constraints for particular acceleration regimes while Figs. 11, 12 represent our updated summary Hillas plots.

The weakest possible constraints (for inductive acceleration with curvature-dominated losses) are presented in Fig. 8. Constraints for inductive acceleration with synchrotron-dominated losses, applicable mostly to inner and outer jets of active galaxies, are given in Fig. 9, while constraints for the most general diffusive acceleration are presented in Fig. 10. Figure 11 represents our version of the Hillas plot with constraints for  $10^{20} \text{ eV}$  protons. Figure 12 is the same plot but for  $10^{20} \text{ eV}$  iron nuclei.

Constraints for neutron stars follow from Sec. 3.1; even for the least restrictive acceleration regime they are not satisfied for UHE particles. In active galaxies, various regimes of acceleration may operate. In the immediate vicinity of the central black hole (up to a few  $R_S$ ), the field configuration allows for the inductive acceleration with curvature-dominated losses. These regions are denoted as “BH” in Figs. 8, 11, 12; the parameters correspond to Eqns. 14 and 11. The latter one is an upper limit on the field, so we extend the boxes for two orders of magnitude lower in  $B$ , cf. Fig. 2. Beyond a few  $R_S$ , the  $\mathbf{E} \parallel \mathbf{B}$  field structure no longer holds, but coherent fields may still be present in inner jets. For these central parsecs of AGN (denoted as “AD” in Figs. 9–12) we use the field estimates from Fig. 1. For the extended parts of active galaxies (jets, jet knots, hot spots and lobes) we use field estimates summarized in Figs. 4, 5. The summary boxes for starburst galaxies include both equipartition and minimal-energy estimates (Fig. 6). For GRB, the summary plots present synchrotron-based estimates for both inner and outer shocks (see Fig. 7 for a more instructive plot). Field estimates for clusters, superclusters and voids follow Sec. 3.5.

The constraints discussed here and expressed in terms of the Hillas plot are necessary, but they should be supplemented by other limits (listed in the beginning of Sec. 2). We note that in estimation of the maximal attainable energy, important constraints are put by interactions of accelerated particles with ambient photons. In particular, interaction with the cosmic microwave background is important for large,  $R \gtrsim \text{Mpc}$ , sources (lobes of radio galaxies, clusters and voids), while interaction with the internal source radiation field is important for ultraluminous sources (GRB and AGN). These constraints, considered elsewhere, further restrict the number of potential UHECR accelerators<sup>3</sup>. For the diffusive shock acceleration, these constraints have been studied e.g. in Ref. [9].

The maximal energy for the supermassive black holes is readily expressed in terms of a single parameter, the black-hole mass  $M_{\text{BH}}$ . We used the upper limit on the magnetic field,  $B_{\text{BH}}$ , which is most likely one or two orders of magnitude higher than the actual values, so that our estimate, Eq. (15), is robust. It depends weakly ( $\sqrt{R/R_S}$ ) on the assumed size of the acceleration region.

While we tried to make all constraints as robust as possible, it is clear that they

---

<sup>3</sup>In certain cases the proton-gamma interactions, instead of pure dissipation, can significantly amplify the acceleration process [19].

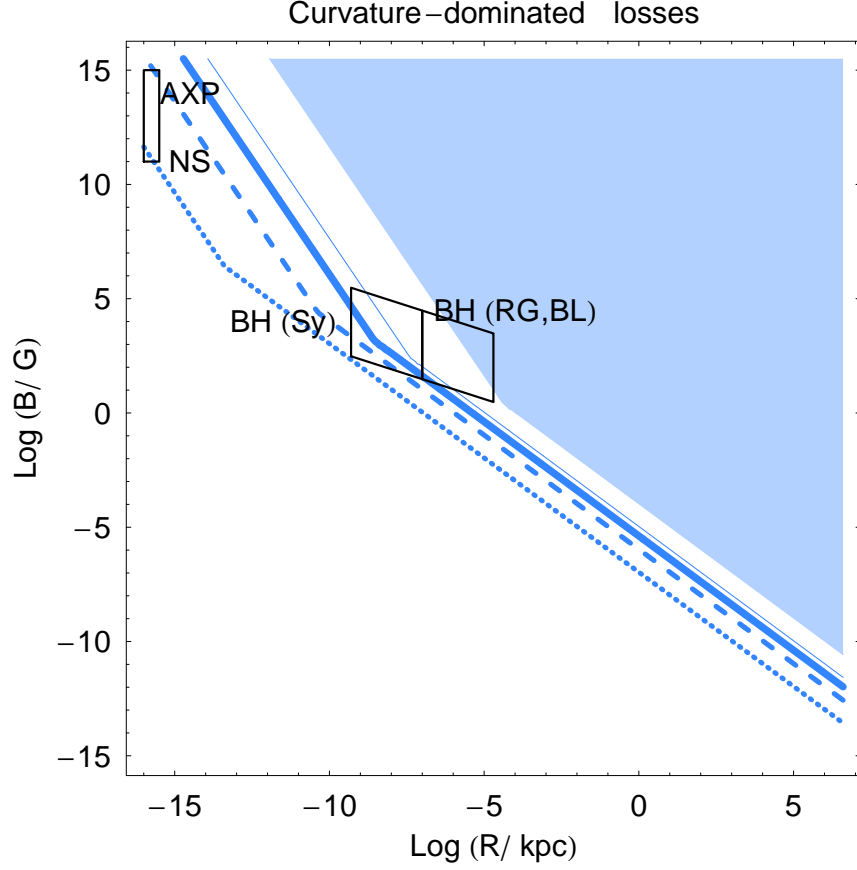


Figure 8: The size-field plot with constraints from geometry and radiation losses for the regime where losses are dominated by curvature radiation. These are minimal possible losses and these constraints are therefore the most weak. Boxes denote parameter regions for objects in which conditions for this loss regime may be satisfied, that is immediate neighbourhood of neutron stars (NS), anomalous X-ray pulsars and magnetars (AXP) and of supermassive central black holes (BH) of active galactic nuclei, from low-power Seyfert galaxies (Sy) to powerful radio galaxies (RG) and blazars (BL). The shaded area corresponds to the parameter region where acceleration of protons to  $10^{20}$  eV is possible. Lines bind from below the allowed regions for  $10^{19}$  eV protons (thin full line),  $10^{20}$  eV iron nuclei (thick full line),  $10^{18}$  eV protons (dashed line) and  $10^{17}$  eV protons (dotted line). Right-hand parts of the lines represent the Hillas constraint while left-hand (steeper) parts represent the radiation-loss constraint.

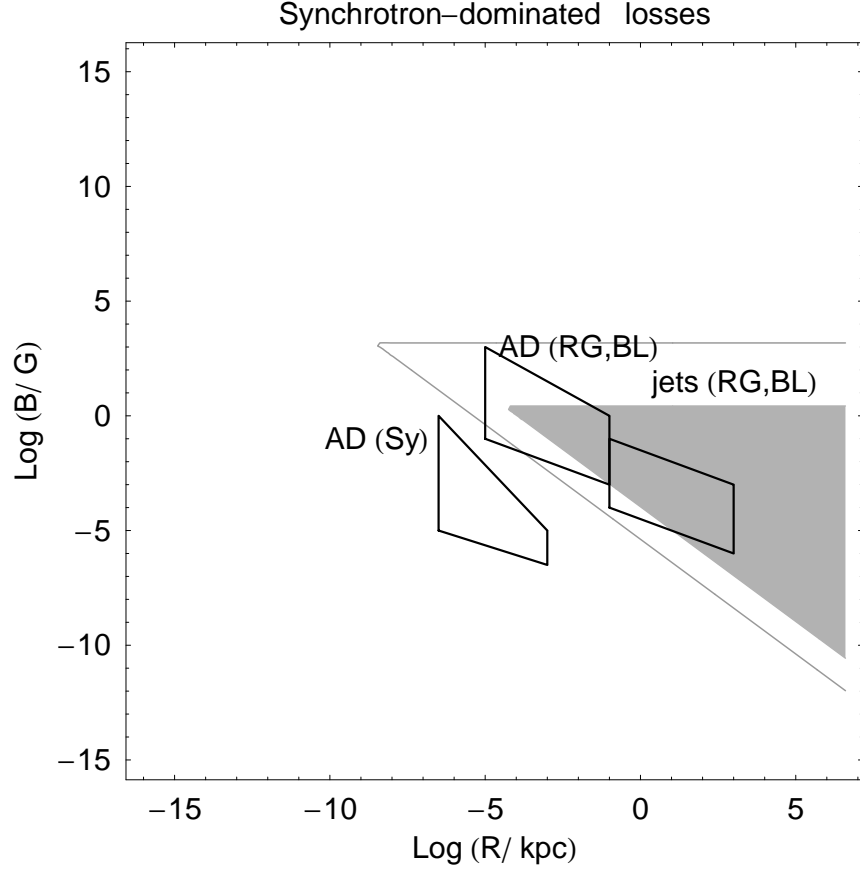


Figure 9: The size-field plot with constraints from geometry and radiation losses for the regime of one-shot acceleration with synchrotron-dominated losses. Boxes denote parameter regions for objects in which conditions for this loss regime may be satisfied, that is central parsecs (AD) of active galaxies (low-power Seyfert galaxies (Sy) and powerful radio galaxies (RG) and blazars (BL)) and relativistic jets of powerful active galaxies. The shaded area corresponds to the parameter region where acceleration of protons to  $10^{20}$  eV is possible. The line binds the allowed regions for  $10^{20}$  eV iron nuclei. Lower lines represent the Hillas constraint while upper (horizontal) lines represent the radiation-loss constraint. All quantities are given in the comoving frame, so the maximal energy for jets should be multiplied by the bulk Lorentz factor of the jet which may be as large as  $\sim 10$  for leptonic jets and  $\sim 100$  for hadronic jets [10].

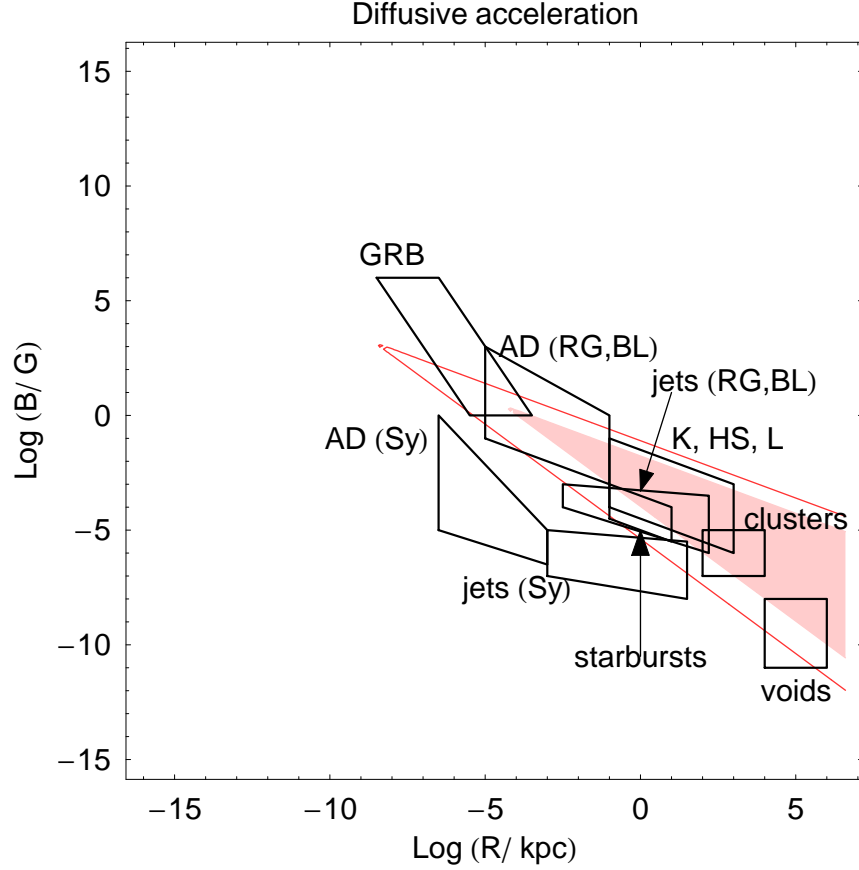


Figure 10: The size-field plot with constraints from geometry and radiation losses for the regime of diffusive acceleration with synchrotron-dominated losses. Boxes denote parameter regions for objects in which conditions for this loss regime may be satisfied, that is central parsecs (AD) of active galaxies (low-power Seyfert galaxies (Sy) and powerful radio galaxies (RG) and blazars (BL)), relativistic jets, knots (K), hot spots (HS) and lobes (L) of powerful active galaxies (RG and BL); non-relativistic jets of low-power galaxies (Sy); starburst galaxies; gamma-ray bursts (GRB); galaxy clusters and intercluster voids. The shaded area corresponds to the parameter region where acceleration of protons to  $10^{20}$  eV is possible. The line binds the allowed regions for  $10^{20}$  eV iron nuclei. Lower lines represent the Hillas constraint while upper lines represent the radiation-loss constraint. All quantities are given in the comoving frame, so the maximal energy for jets and shells of GRBs should be multiplied by the bulk Lorentz factor which may be as large as  $\sim 10$  for leptonic jets and  $\sim 100$  for hadronic jets and GRBs [10].

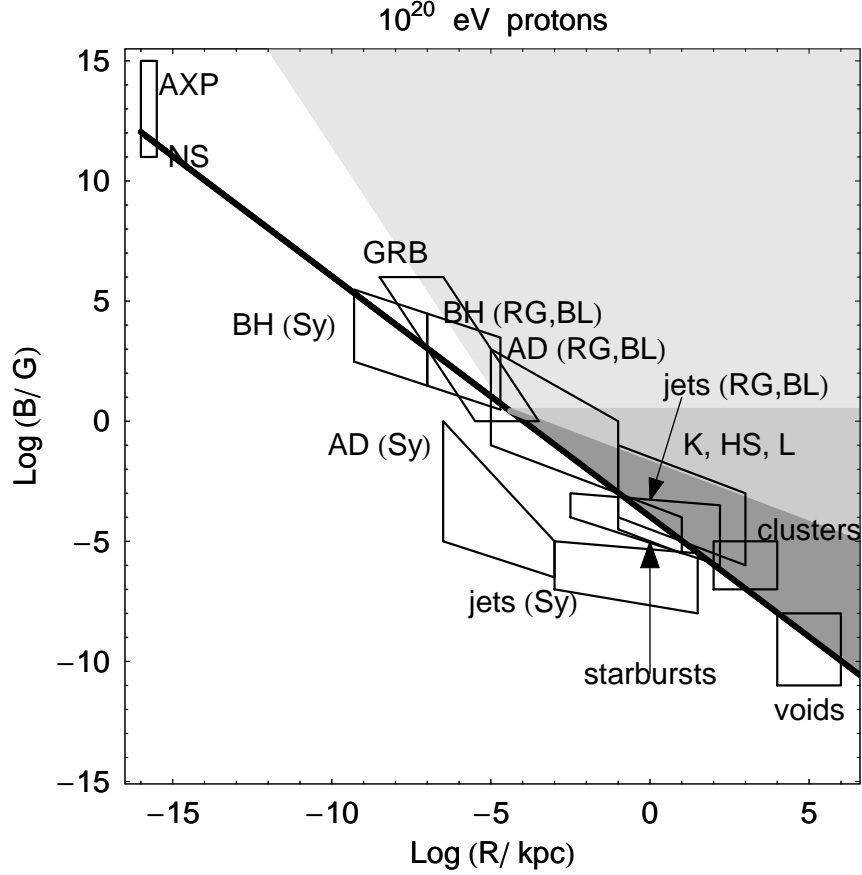


Figure 11: The Hillas plot with constraints from geometry and radiation losses for  $10^{20}$  eV protons. The thick line represents the lower boundary of the area allowed by the Hillas criterion. Shaded areas are allowed by the radiation-loss constraints as well: light grey corresponds to one-shot acceleration in curvature-dominated regime only; grey allows also for one-shot acceleration in synchrotron-dominated regime; dark grey allows for both one-shot and diffusive (e.g. shock) acceleration. See captions to Figs. 8, 9, 10 for notation of boxes corresponding to potential sources.

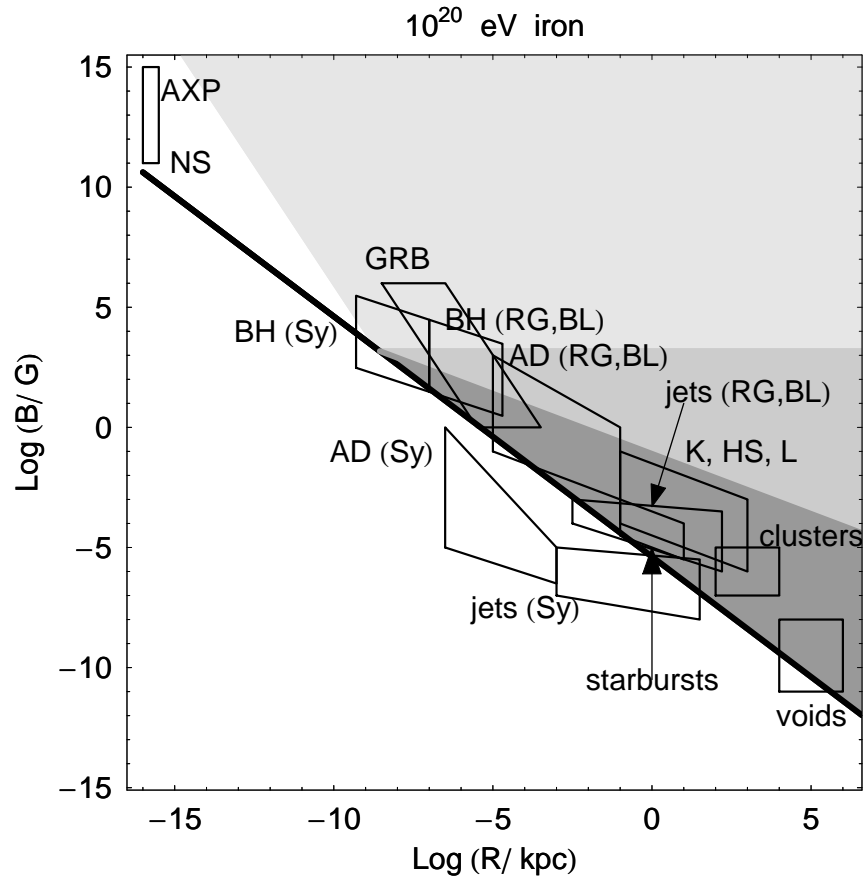


Figure 12: The same as Fig. 11 but for  $10^{20}$  eV iron nuclei. The most important difference with Fig. 11 is that acceleration of iron nuclei to  $10^{20}$  eV is possible (unlike for protons) in low-power active galaxies (e.g. Seyfert galaxies).

should be considered as order-of-magnitude estimates (in fact, typical precision of the magnetic-field determination is an order of magnitude) and, for individual unusual field configurations, can be quantitatively violated. An example of such a configuration is a linear accelerator with curvature radius  $r$  of field lines exceeding the size of the source  $R$ ; then  $R$  should be substituted by  $r$  in Eq. (9). The estimates should be used with care for the cases when the magnetic field changes violently within the accelerator (for instance when particles are accelerated by magnetic reconnection). A more detailed modelling of acceleration and losses is required in these cases.

One of our most important conclusions is that low-power active galaxies (e.g. Seyfert galaxies) cannot accelerate protons to energies  $\gtrsim 5 \times 10^{19}$  eV. Indeed, when the extended structures (jets and outflows) are present, the magnetic field there is far too weak to satisfy the Hillas condition (even for very rare relativistic jets), see Fig. 4. The same is true for the accretion disks, where the field is nicely constrained from above by non-observation of the Zeeman splitting in megamasers (Fig. 1). The most favourable conditions for acceleration correspond to the immediate vicinity (a few  $R_S$ ) of the central black hole where the upper limit on the maximal energy is given by Eq. (15). Since for Seyfert galaxies,  $M_{\text{BH}} \lesssim (10^7 \div 10^8) M_\odot$ , proton acceleration to  $\sim 10^{20}$  eV is not allowed. However, these (and only these) central parts of Seyfert galaxies can, in principle, accelerate protons to  $\sim 10^{18}$  eV and heavy nuclei to  $\sim 10^{20}$  eV, if interactions with ambient photons are weak enough. Though heavy nuclei are much less abundant than protons, Seyfert galaxies themselves are much more abundant, and hence typically close to the observer, than powerful radio galaxies and blazars, so that their population can contribute to the UHECR spectrum.

## 5 Conclusions

We reviewed constraints on astrophysical UHE accelerators and presented the Hillas plot supplemented with radiation-loss constraints and updated with recent astrophysical data. Contrary to previous studies, we emphasised that active galaxies span a large area on the plot, and only the most powerful ones (radio galaxies, quasars and BL Lac type objects) are capable of acceleration of protons to UHE. If UHECR particles are accelerated close to the supermassive black holes in AGN, then most likely the mechanism is “one-shot” with energy losses dominated by the curvature radiation. Other potential UHE acceleration sites are jets, lobes, knots and hot spots of *powerful* active galaxies, starburst galaxies and shocks in galaxy clusters. Acceleration of particles in supercluster-scale shocks, gamma-ray bursts and inner part of AGN is subject to additional constraints from  $p\gamma$  interactions which are not discussed here.

Unlike protons, heavy nuclei can be accelerated to UHE in circumnuclear regions of low-power active galaxies. Since these galaxies are abundant, this contribution to UHECR flux may be important, leading to a mixed primary cosmic-ray composition at highest energies.

The authors are indebted to D. Gorbunov, S. Gureev, A.M. Hillas, V. Lukash, A. Neronov, S. Popov and D. Semikoz for interesting discussions. We acknowledge the use of online tools [53, 54]. This work was supported in part by the grants RFBR 07-02-00820 09-07-08388 (ST), NS-1616.2008.2 (ST) and by FASI government contracts 02.740.11.0244 (ST) and 02.740.11.5092 (KP, ST) and by the Dynasty Foundation (KP, ST).

## A Derivation of electrodynamic results

### A.1 Energy losses for the curvature radiation (see e.g. Ref. [88])

Consider a particle moving along curved field lines. The particle has a longitudinal velocity component ( $\mathbf{v}_{\parallel} \parallel \mathbf{B}$ ) and a drift component ( $\mathbf{v}_d \perp \mathbf{B}$ ). This drift component provokes the appearance of the Lorentz force which curves the particle's trajectory towards the field lines. For a relativistic particle,

$$v_d = \frac{v_{\parallel}^2 m}{qBr} \left( \frac{\mathcal{E}}{m} \right),$$

so the Lorentz force is

$$\mathbf{F}_L = q[\mathbf{v}_d \times \mathbf{B}],$$

$$F_L = \frac{v_{\parallel}^2 m}{r} \left( \frac{\mathcal{E}}{m} \right).$$

The energy losses are in general determined by Eq. (5) which may be rewritten as

$$\frac{d\mathcal{E}}{dt} = \frac{2q^2}{3m^2(1-v^2)} \left[ F^2 - (\mathbf{F} \cdot \mathbf{v})^2 \right].$$

In the regime we consider,  $(\mathbf{F} \cdot \mathbf{v}) = 0$  and consequently

$$\frac{d\mathcal{E}}{dt} = \frac{2q^2 v_{\parallel}^4}{3r^2} \left( \frac{\mathcal{E}}{m} \right)^4.$$

In the ultrarelativistic limit  $v_{\parallel} \rightarrow c$  one obtains Eq. (9).

### A.2 The maximal energy for diffusive acceleration [11]

Consider a flow propagating through a magnetized medium. An accelerated particle gains energy by repeated scattering off the flow. After every scattering, the particle travels along the Larmor orbit, radiates and slows down according to Eq.(6); consequently

$$\int_{\mathcal{E}_0}^{\mathcal{E}} \frac{d\mathcal{E}}{\mathcal{E}^2} = -\frac{2q^4}{3m^4} \int_0^R B^2(x) dx,$$

hence

$$\frac{1}{\mathcal{E}} = \frac{1}{\mathcal{E}_0} + \frac{2q^4}{3m^4} \int_0^R B^2(x) dx.$$

The maximal energy  $\mathcal{E} = \mathcal{E}_{\text{cr}}$  is determined by setting  $\mathcal{E}_0 \rightarrow \infty$ ,

$$\frac{1}{\mathcal{E}_{\text{cr}}} = \frac{2q^4}{3m^4} \int_0^R B^2(x) dx \simeq \frac{2q^4}{3m^4} B^2 R,$$

and we obtain Eq. (7).

## References

- [1] Nagano M and Watson A A, *Observations And Implications Of The Ultrahigh-Energy Cosmic Rays*, 2000, *Rev. Mod. Phys.* **72** 689
- [2] Kachelriess M, 2008, arXiv:0801.4376 [astro-ph]
- [3] Greisen K, 1966 *Phys. Rev. Lett.* **16** 748
- [4] Zatsepin G T and Kuzmin V A, 1966 *JETP Lett.* **4** 78
- [5] Abbasi R *et al.*, (The High Resolution Fly’s Eye Collaboration), 2008, *Phys. Rev. Lett.* **100** 101101
- [6] The Pierre Auger Collaboration, 2008, arXiv:0806.4302 [astro-ph]
- [7] Schlüter A und Biermann L, 1950, *Z. Naturforsch.* **5a** 237
- [8] Hillas A M, 1984, *Ann. Rev. Astron. Astrophys.* **22** 425
- [9] Protheroe R J, 2004, *Astropart. Phys.* **21** 415
- [10] Aharonian F A, 2002, *Phys. Rev.* **D66** 023005
- [11] Medvedev M V, 2003, *Phys. Rev.* **E67** 045401
- [12] Gureev S and Troitsky S, arXiv:0808.0481 [astro-ph]
- [13] Kachelriess M and Semikoz D V, 2006 *Phys. Lett.* **B634** 143
- [14] Landau L and Lifshitz E, *The classical theory of fields*, 1951, Addison–Wesley
- [15] Longair M S, *High-energy astrophysics. Vol. 1: Particles, photons and their detection*, 1992, Cambridge Univ. Press
- [16] Fermi E, 1949 *Phys. Rev.* **75** 1169
- [17] Blandford R and Eichler D, 1987 *Phys. Rept.* **154** 1
- [18] Rieger F M and Duffy P, 2004 *Astrophys. J.* **617** 155
- [19] Derishev E V, Aharonian F A, Kocharovskiy V V and Kocharovskiy V I V, 2003 *Phys. Rev. D* **68** 043003
- [20] Ostrowski M, 2008, arXiv:0801.1339 [astro-ph]
- [21] Schopper R, Birk G T and Lesch H, 2001 *Astropart. Phys.* **17** 347
- [22] Venkatesan A, Miller M C and Olinto A V, 1997 *Astrophys. J.* **484** 323
- [23] Neronov A and Semikoz D, 2003 *New Astron. Rev.* **47** 693
- [24] Neronov A, Tinyakov P and Tkachev I, 2005 *J. Exp. Theor. Phys.* **100** 656
- [25] Neronov A, Semikoz D and Tkachev I, 2007, arXiv:0712.1737 [astro-ph]
- [26] Torres D F and Anchordoqui L A, 2004 *Rept. Prog. Phys.* **67** 1663 [arXiv:astro-ph/0402371]
- [27] Gorbunov D and Troitsky S, 2005 *Astrop. Phys.* **23** 175
- [28] Giovannini M, 2004 *Int. J. Mod. Phys. D* **13** 391
- [29] Vallée J P, 2004, *New Astron. Rev.* **48** 763
- [30] Mereghetti S, arXiv:0804.0250 [astro-ph]
- [31] Bignami G F *et al.*, 2003 *Nature* **423** 725
- [32] Baring M G and Harding A K, 2007 *Astrophys. Space Sci.* **308** 109

- [33] Carroll B W and Ostlie D A, *An introduction to modern astrophysics*, 2007, Pearson/Addison Wesley
- [34] Zasov V A and Postnov K A, *General astrophysics*, 2006, Vek-2 (in Russian)
- [35] Véron-Cetty M P and Véron P, 2000 *Astron. Astrophys. Rev.* **10** 81
- [36] Fanaroff B L and Riley J M, 1974 *Mon. Not. Roy. Astron. Soc.* **167** 31P
- [37] Vlemmings W H T, Bignall H E and Diamond P J, 2007 *Astrophys. J.* **656** 198
- [38] Modjaz M *et al.*, J. M. Moran J M, Kondratko P T and Greenhill L J, 2005 *Astrophys. J.* **626** 104
- [39] McCallum, J N, Ellingsen S P, Lovell J E J, 2007 *Mon. Not. Roy. Astron. Soc.* **376** 549
- [40] Zavala R T and Taylor G B, 2002 *Astrophys. J.* **566** L9
- [41] Matveenko L I *et al.*, 1980, *Sov. Astron. Lett.* **6** 42
- [42] Artyukh V S and Chernikov P A, 2007 *Astron. Rep.* **51** 808
- [43] Tyul'bashev S A, 2005, *Astron. Rep.* **49** 967
- [44] Chernikov P A *et al.*, 2006 *Astron. Rep.* **50** 202
- [45] Sligh V I, 1963 *Nature* **199** 682
- [46] Zakharov A F *et al.*, 2003 *Mon. Not. Roy. Astron. Soc.* **342** 1325
- [47] Gnedin Y M, Natsvlishvili T M and Piotrovich M Y, 2005 *Grav. Cosmol.* **11** 333
- [48] Znajek R L, 1978 *Mon. Not. Roy. Astron. Soc.* **185** 833
- [49] Ghosh P and Abramowicz M A, 1997 *Mon. Not. Roy. Astron. Soc.* **292** 887
- [50] Shakura N I and Syunyaev R A, 1973 *Astron. Astrophys.* **24** 337
- [51] Novikov I D and Thorne K S, 1973, in: *Black holes (Les astres occlus)*, Gordon and Breach, p. 343
- [52] Zhang W M, Lu Y and Zhang S N, 2005 *Chin. J. Astron. Astrophys. Suppl.* **5** 347
- [53] Paturel G *et al.*, 2003 *Astron. Astrophys.* **412** 45; <http://leda.univ-lyon1.fr>
- [54] The NASA/IPAC Extragalactic database (available at <http://nedwww.ipac.caltech.edu>).
- [55] Harris D E and Krawczynski H, 2006 *Ann. Rev. Astron. Astrophys.* **44** 463
- [56] Gallimore J F *et al.*, 2006 *Astron. J.* **132** 546
- [57] Schurch N J, Roberts T P and Warwick R S, 2002 *Mon. Not. Roy. Astron. Soc.* **335** 241
- [58] Kataoka J *et al.*, 2006 *Astrophys. J.* **641** 158
- [59] Hardcastle M J *et al.*, 2007 *Astrophys. J.* **670** L81
- [60] Allen, M G *et al.*, 1999 *Astrophys. J.* **511** 686
- [61] Laine S and Beck R, 2008 *Astrophys. J.* **673** 128
- [62] Burns J O, Feigelson E D, Schreier E J, 1983 *Astrophys. J.* **273** 128
- [63] Schwartz D A *et al.*, 2003 *New Astron. Rev.* **47** 461
- [64] Hardcastle M J, Harris D E and Worrall D M, 2004 *Astrophys. J.* **612** 729
- [65] Harris D E *et al.*, arXiv:0904.3925

- [66] Kataoka, J and Stawarz, L, *Astrophys. J.* **622** 797
- [67] Meisenheimer K *et al.*, 1989 *Astron. Astrophys.* **219** 63
- [68] Croston J H *et al.*, 2005 *Astrophys. J.* **626** 733 [arXiv:astro-ph/0503203].
- [69] Vlemmings W H T *et al.*, arXiv:astro-ph/0510452.
- [70] Slysh V I and Migenes V, 2006 *Mon. Not. Roy. Astron. Soc.* **369** 1497
- [71] Vlemmings W H T, 2008 *Astron. Astrophys.* **484** 773
- [72] Sarma A P *et al.*, 2008 *Astrophys. J.* **674** 295
- [73] Curran R L and Chrysostomou A, 2007 *Mon. Not. Roy. Astron. Soc.* **382** 699
- [74] Anchordoqui L A, Romero G E and Combi J A, 1999 *Phys. Rev. D* **60** 103001
- [75] Thompson T A *et al.*, 2006 *Astrophys. J.* **645** 186
- [76] Piran T, 2005 *AIP Conf. Proc.* **784** 164
- [77] Lyutikov M, *Magnetic fields in GRBs*, arXiv:astro-ph/0409489.
- [78] Piran T, 1999 *Phys. Rept.* **314** 575
- [79] Govoni F and Feretti L, 2004 *Int. J. Mod. Phys. D* **13** 1549
- [80] Ferrari C *et al.*, 2008 *Space Science Reviews*, **134** 93
- [81] Beck R and Krause M, 2005 *Astron. Nachr.* **326** 414
- [82] Kronberg P P, Kothes R, Salter C J and Perillat P, 2007 *Astrophys. J.* **659**, 267
- [83] Clarke T E, Kronberg P P and Boehringer H, 2001 *Astrophys. J.* **547** L111
- [84] Taylor G B *et al.*, 2006 *Mon. Not. Roy. Astron. Soc.* **368** 1500
- [85] Govoni F *et al.*, 2006 *Astron. Astrophys.* **460** 425
- [86] Dolag K *et al.*, 2005 *JCAP* **0501** 009
- [87] Sigl G, Miniati F and Ensslin T A, 2004 *Nucl. Phys. Proc. Suppl.* **136** 224
- [88] Ginzburg V L, Syrovatskii S I, *The origin of cosmic rays*, 1964, London: Pergamon Press